INSTITUT DE FRANCE
Académie des sciences

# Comptes Rendus
# Mécanique

Filip Nikolić and Marko Čanađija

**Deep Learning of Temperature – Dependent Stress – Strain Hardening Curves**

Volume 351 (2023), p. 151-170

Published online: 12 May 2023

https://doi.org/10.5802/crmeca.185

This article is licensed under the
Creative Commons Attribution 4.0 International License.
http://creativecommons.org/licenses/by/4.0/

*Les* Comptes Rendus. Mécanique *sont membres du*
*Centre Mersenne pour l'édition scientifique ouverte*
www.centre-mersenne.org
e-ISSN : 1873-7234

*Comptes Rendus*
*Mécanique*
**2023**, Vol. 351, p. 151-170
https://doi.org/10.5802/crmeca.185

Spontaneous articles / *Articles spontanés*

# Deep Learning of Temperature – Dependent Stress – Strain Hardening Curves

**Filip Nikolić** [a, b] **and Marko Čanađija** [*, a]

[a] University of Rijeka, Faculty of Engineering, Department of Engineering Mechanics, Vukovarska 58, 51000 Rijeka, Croatia

[b] Elaphe Propulsion Technologies Ltd, CAE Department, Litostrojska 44c, 1000 Ljubljana, Slovenia

*E-mails:* fnikolic@riteh.hr (F. Nikolić), marko.canadija@riteh.hr (M. Čanađija)

**Abstract.** In this study, structure – property relationships (SPR) have been investigated using machine learning methods (ML). The research objective was to create a ML model that can predict the stress – strain response of materials at different temperatures from a given microstructure with industrially acceptable accuracy and high computational efficiency. Automated microstructure generation techniques and numerical simulations were developed to create a dataset for the ML model. Two – phase 3D representative volume elements (RVEs) were analyzed using finite element analysis (FEA) to obtain the stress – strain responses of the RVEs. The phase arrangement of the RVEs, the temperature, and the stress – strain responses were used to train the ML model. The microstructure arrangement and the temperature – dependent mechanical properties of each phase were known parameters, while the output parameter was the stress – strain response of the two – phase RVE. The ML model has shown excellent prediction accuracy in the temperature range from 20 °C to 250 °C. In addition, the model showed very high computational efficiency compared to FEA, allowing much faster prediction of the stress – strain curves at specific temperatures.

**Keywords.** deep learning, temperature dependent stress – strain curves, structure – property relationships, finite element analysis, machine learning.

**Funding.** This work was supported in part by the University of Rijeka under project number uniri-tehnic-18-37 and in part by the Croatian Science Foundation under project IP-2019-04-4703.

**Electronic supplementary material.** The raw data required to reproduce the present study consist of the trained CNN and the dataset for the random temperature levels described in the Results and Discussion section. It should be noted that the full dataset is not included due to very large memory size. Data are available for download on the Mendeley Data: Nikolic, Filip (2022), "Dataset and CNN", Mendeley Data, V1, doi: 10.17632/z8d9s7g5sz.1.

*Manuscript received 19 October 2022, revised 13 February 2023, accepted 6 March 2023.*

* Corresponding author.

## 1. Introduction

It is well-known that mechanical properties are one of the most important factors in material selection. Accurate material properties are very important in the product development phase to virtually design the product to withstand its in – service life due to external loads. Mechanical properties are often difficult to determine, and this problem is exacerbated for temperature – dependent properties. For applications at temperatures different from room temperature, it is often difficult to obtain accurate mechanical properties, especially the complete stress – strain curve. In addition, for most engineering applications, the mechanical properties at room temperature may not describe the problem accurately enough. If the material is heterogeneous, the property of interest is related to the arrangement of the phases and the properties of individual phase [1]. There are a variety of methods for determining mechanical properties, but the structure – property relationships (SPR) should be the most accurate. SPR could be established via different approaches as analytical and numerical approach, statistical continuum theories, etc. [2]. It is also known that it is more representative to model SPR problem on a 3D scale than on a 2D scale. Moreover, although SPR task is very useful, it is also often too time consuming to apply it in a design process.

As in mechanical engineering and computational materials science, this topic is also very attractive in many other disciplines such as pharmacy, medicine, physics, chemistry, optics, and more. Even though a SPR can be obtained by various methods, the preferred choice in recent decades is finite element analysis (FEA). Although there is a tremendous amount of research on this topic, the number of studies on the temperature influence is much smaller. In general, the drawback of these methods is that the computational cost is relatively high, so adoption by industry can be difficult. In solving the problem of computational inefficiency, machine learning (ML) methods could be of great use. For example, research [2] pointed out the computational efficiency of the ML model which made 1000 predictions in 0.2 seconds on a personal desktop computer. At the same time, a single FEA simulation on the same problem took 15 to 46 minutes on average.

Recently, some studies have been conducted to determine SPR using ML techniques. Zhang et al. [3] proposed a SPR model based on the least squares method and a relatively simple artificial neural network (ANN) structure. Jung et al. [2] performed microstructure – based simulations for 1 100 different synthetic microstructures to predict the elongation, ultimate tensile strength, and strain localization index defined in the soft phase of each microstructure. They also used dimensionality reduction techniques such as principal component analysis (PCA) and multidimensional scaling (MDS). The most important feature of the dimensional reduction techniques is that it could reduce the model size and computational cost, but it could also reduce the model accuracy. After some evaluation, the authors concluded that the MDS outperforms PCA in establishing lower dimensional representation of the microstructure. Latypov and Kalidindi [4] calibrated the data – driven links with FEA results on a large ensemble of digitally created microstructures. They also used PCA techniques for dimensionality reduction. They reduced the 3D $27\times27\times27$ microstructure into a 2D microstructure projection by applying PCA. Yang et al. [5] predicted the macroscale elastic properties of a high – contrast composite based on its microstructural information using ML. They showed that the convolutional neural network (CNN) developed in their study outperformed all comparative methods. Cecen et al. [6] employed a 3D CNN to learn the features of material microstructures that lead to good prediction performance for the effective property of interest. They also used PCA for dimension reduction. For dimensionality reduction method, they used regression and the 10-fold cross validation scheme. Wang et al. [7] demonstrated the application of a ML approach to correlate SPR in polymer nanocomposites. Liu et al. [8] proposed the deep material network transfer learning strategy for SPR predictions.

Kotha et al. and Frankel et al. [9, 10] also used complex ML algorithms to predict material constitutive models based on SPR. However, from the above, it can be concluded that none of these authors considered the temperature dependence of the observed property and also did not predict complete stress – strain curves, which could be important for many engineering applications. In addition, most authors used dimension reduction techniques to reduce input size of the model, but as already discussed this can affect accuracy.

Additionally, there are some studies dealing with the prediction of stress – strain curves via ML. Yang et al. [11] predicted stress – strain curves of composite materials using CNN, however, their study is based on a two – dimensional geometry. Jiang et al. [12] predicted the stress – strain response of the fiber reinforced polymer confined concrete using ML. Anyhow, their ML model do not directly takes into account the microstructural arrangement. Wen et al. [13] predicted temperature and time – dependent deformation in lithium metal using ML model. They also did not take into account the microstructural informations and investigated metal was not dual – phase material. Versino et al. [14] developed a ML model to predict a material constitutive model for a different strain rates and temperatures not taking into account microstructural informations. Kronberger et al. [15] presented an approach to calibrate material properties from processing conditions based on genetic programming. Their work included temperature dependency of the properties. In addition, there is an enormous number of research dealing with prediction of material constitutive model via ML and not all of them could be discussed herein.

Although there are some recent studies dealing with SPR via ML [1–8, 11, 16–24], none of them directly predicted the stress – strain curves based on the microstructural arrangement that takes into account the influence of temperature variations on the evaluated property. The evaluation of the temperature dependence of the stress-strain curves from the classical finite element analysis of the microstructure can be found in the literature. However, to the best of the author's knowledge, there is no study describing the determination of temperature dependent stress–strain curves using machine learning techniques.

## 2. Methods

### 2.1. *Microstructure Generation*

To obtain SPR of a material, a large number of different microstructures should be generated. In the present study, equiaxed 3D two – phase microstructures consisting of 26×26×26 voxels representing representative volume elements (RVEs) were generated using the open – source software Dream.3D [25]. With a similar size of microstructures, other authors [2, 4] have obtained excellent results, so in this study the dimensions 26×26×26 were adopted. Although many authors choose to model the SPR problem on a 2D scale [1, 7, 8, 22, 23, 26–29], mainly because of the better computational efficiency, this research presents SPR incorporation on the 3D scale, because it is more consistent with the physical material behavior. It is important to obtain a wide range of possible arrangements of phases in the microstructure because the properties depend on them. A Python script was used to automate the creation of the dataset. Due to the Gaussian random distribution in the generation of the microstructure in the software, only the volume fractions of the phases were changed, ranging in this example from 0% to 15% and 85% to 100% of the second (hard) and first (soft) phase, respectively. Thus, the results will also show the mechanical behavior of weaker material reinforced by a small proportion of strong material. The grain size in Dream.3D is described by the average value of the lognormal grain size distribution and the standard deviation of the lognormal grain size distribution and the values of 3 and 0.25 were used, respectively. For more information, see [25]. For the simplicity, all other parameters were kept constant. The parameters resulted in hard phase particle sizes from 2 mm to 13 mm

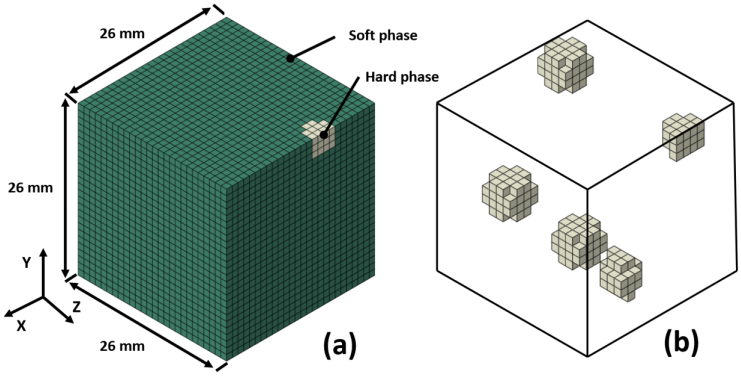


**Figure 1.** A random RVE arrangement: dimensions and example of phases arrangement: (a) soft and hard phase within the whole RVE and (b) arrangement of the hard phase within the RVE

and the amount of from 1 to 15 hard phase particles. The particles were randomly distributed within the microstructure. In addition, the mean of the distribution of the hard phase was 0.067, while the standard deviation of the hard phase was 0.036. The both of the phases were the of hexagonal close – packed type. The resulting database consists of 2977 different RVEs. Additional details about microstructure generation using Dream.3D software, an interested reader could find in [25]. In addition, an example of a random microstructure configuration is showed in Fig. 1.

It should be emphasized that the considered microstructure is not intended to realistically model some particular material. This is a standard approach in this kind of research, see for example [2, 6, 8, 11]. Nevertheless, although of an academic nature, it still resembles a typical microstructure. As such, it demonstrates that the computational procedure proposed in this research can be also applied to realistic microstructures. Note that high fidelity microstructures can be created by resorting to generative adversarial networks, as shown in [30]. Starting from two-dimensional micrographs, a 3D representation of multiphase material can be generated. Although development of such microstructure is beyond of the present research, it can be readily included in the computational procedure proposed here.

## 2.2. *Dataset Generation*

The output of Dream.3D is a random arrangement of the first and second phases mapped onto the discretized finite element mesh consisting of 26×26×26 elements. Thus, the finite element mesh and the arrangement of the phases match in dimension and size. Examples of the mesh and the dimensions of the RVE are shown in Fig. 1. Each element was assigned the properties of the first or the second phase, depending on the arrangement of the phases obtained from Dream.3D. A Young's modulus of 50 and 500 GPa was used for the first and second phases, respectively, while a Poisson's ratio of 0.33 was used for both phases. For simplicity, both Poisson's ratio and Young's modulus values were held constant at the temperature variations used in this study. The temperature – dependent true plastic strain properties of both phases are modelled as piecewise linear curves and are shown in Fig. 2. This mean that the plasticity is modelled as a piecewise linear hardening. In addition, the constitutive model includes softening (e.g. lowering of the yield and ultimate tensile stress of the material with increasing temperature). As in another studies [2, 6, 8, 11], the phases are generic and it was not intended to reproduce

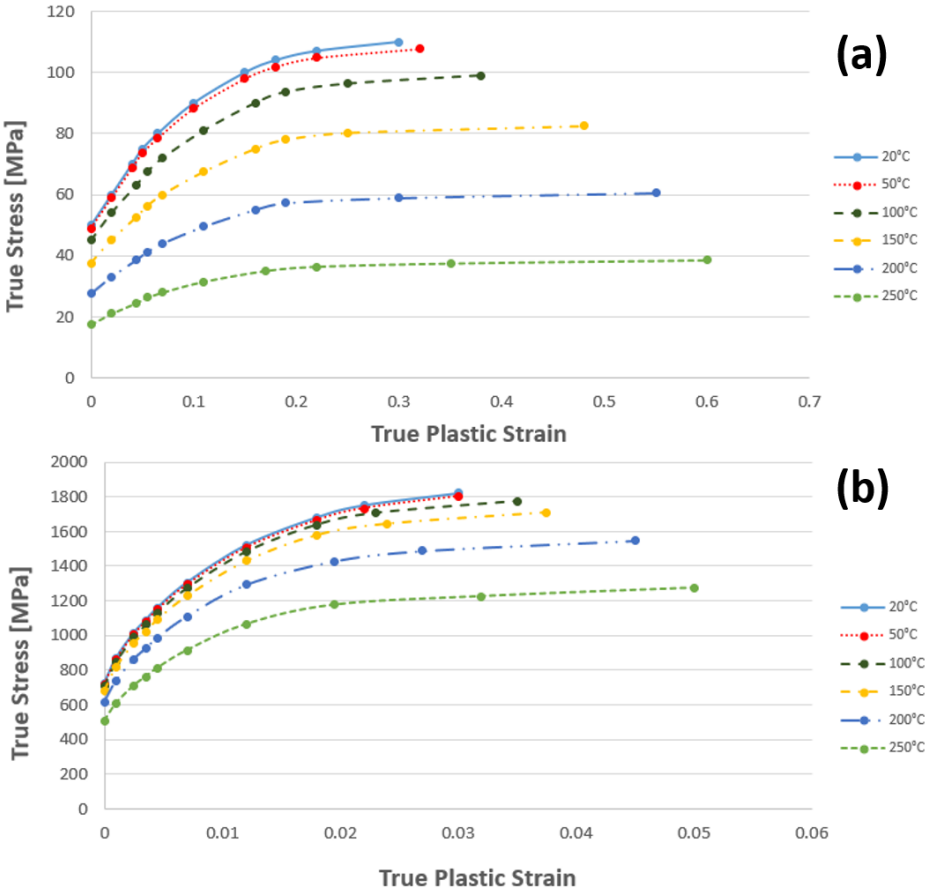


**Figure 2.** Temperature dependent true stress – true plastic strain diagrams of (a) soft and (b) hard phase of the microstructure

real stress-strain curves. However, the soft phase has similar material properties to an aluminum or magnesium alloy, while the material properties of the hard phase could fall into the range of high-strength steel or some synthetic ceramics. The lower flow curves are associated with the higher temperatures. Thus, the arrangement of the phases within the RVE and the temperature – dependent true stress – true strain responses of each phase are the only variable parameters.

Abaqus version 2021 software was used for the numerical simulations of the RVEs. Nonlinear material behavior using incremental plasticity, large displacement, and nonlinear geometric behavior was used to solve the analysis. The von Mises yield surface is used to define isotropic yielding. It is defined by giving the value of the uniaxial yield stress as a function of uniaxial equivalent plastic strain and temperature i. e. the constitutive model is specified as a set of points with the yield stress, equivalent plastic strain and temperature as coordinates. The set is graphically presented in Fig. 2. The mesh was discretized by first – order hexahedral incompatible modes C3D8I elements with eight nodes and four integration points from the Abaqus standard element library. These elements were chosen to overcome issues related to the isochoric nature of plasticity in metals while maintaining computational efficiency in contrast to second – order elements. Phases are connected in a way that nodes between neighbor elements are shared. All analyzes were solved with 20 uniformly spaced time increments to keep the output for the ML model constant. Periodic boundary conditions were applied following the procedures in [31–33].

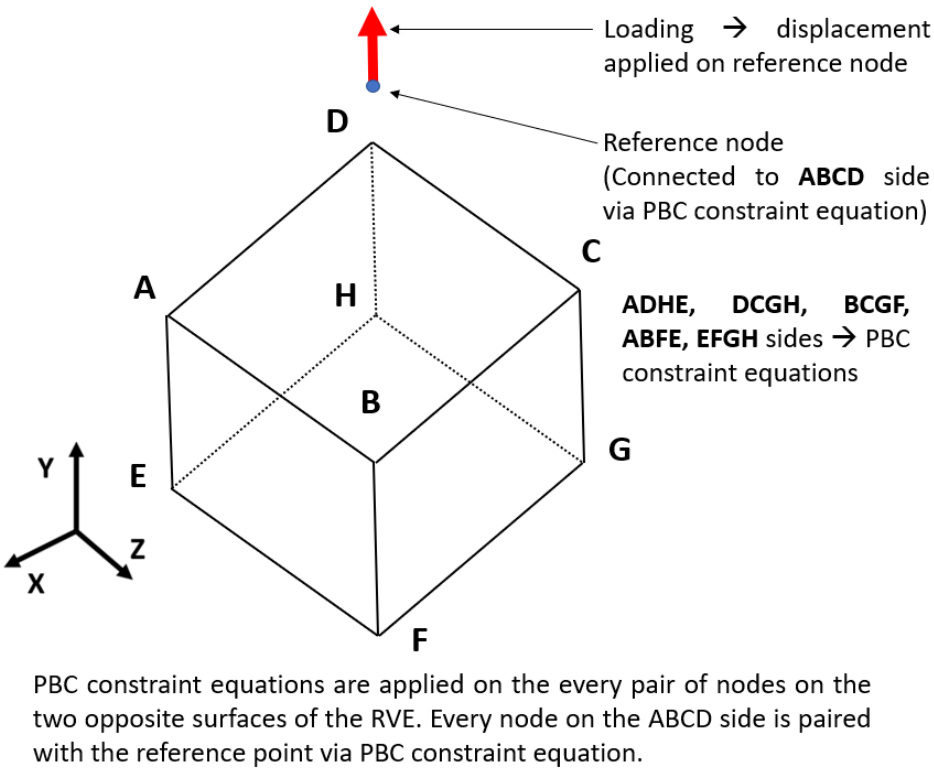


**Figure 3.** Simplified sketch of the application of PBC to the RVE

The loading was applied in the form of displacement in Y axis direction on reference point (as described in [31]) with a strain magnitude of 0.57%, Fig. 3. Thus the proposed boundary conditions results for the material state as in the uniaxial tensile tests. The analysis was considered as an uncoupled thermomechanical analysis with predefined temperature field. Therefore, the temperature was kept constant during an analysis. The implicit Abaqus Standard solver was used, with simulation completion taking between 7 and 32 minutes, or on average 15 minutes, depending on the RVE arrangement and temperature. Default Abaqus implicit solver convergence criterions were adopted to solve the analysis and one could find them in [34]. It took 480 hours to create the entire dataset by FEA. At higher temperatures, the slope of the true stress – true strain response was lower, making convergence more difficult to achieve. Therefore, simulation time increased with increasing temperature. All simulations were computed on a personal desktop computer with an Intel®Core$^{TM}$ I7 – 4970 CPU and a single processing unit. In addition, the creation of the finite element models was automated using Python scripts. In the absence of experimental results, it is assumed that the material behavior is reasonably captured by FEA.

As mentioned before, the considered strain is rather low. The reason for this is the computational cost. In particular, several simulations were performed with a higher strain magnitude. However, when using an implicit solver, this led to convergence problems at temperatures of 150 °C and higher, which were resolved by using smaller increments. Thus, the computational cost increases for two reasons: higher strain magnitude and a larger number of increments. Considering that 3000 simulations need to be performed, the cost per simulation becomes prohib-

itively expensive with present computational resources. Alternatively, an explicit solver could overcome the convergence problems, but this turned out to be even more computationally expensive as the simulation time increased to more than 7 h on a single RVE. Thus, it was not possible to investigate the phenomena that occur at higher strains while running a large number of simulations in a realistic time period.

Simulations were performed at six different temperature levels: 20 °C, 50 °C, 100 °C, 150 °C, 200 °C, and 250 °C. The number of simulations performed at each temperature level are listed in Table 1. It should be noted that 500 microstructures were initially created for each of six temperature levels. From these, 23 did not achieve convergence within the specified fixed number of increments and were therefore disregarded, so, 2977 different microstructures were considered in total. This number of microstructures as well as the size of the microstructure is in the line with other studies on similar 3D problems [2, 4, 5]. For each temperature level, the arrangement of phases is visualized for a random RVE, Fig. 4. For the RVE in Fig. 4, the resulting true von Mises stress, total displacement, and true equivalent plastic strain are shown for the corresponding RVEs, Figs. 5, 6, 7. It should be noted that deformation was scaled by 25 × in all three figures. The true equivalent plastic strain describes the inelastic deformation of the material and corresponds to the PEEQ Abaqus output [34]. At higher temperature values, as well as at a lower fraction of the hard phase, the average stress values of the RVE were lower. The non – uniformity of total displacement was strongly correlated to the higher fraction of hard phase. Moreover, the higher the fraction of hard phase, the higher was the average value of the true equivalent plastic strain, while it did not depend on the temperature.

**Table 1.** Number of simulation performed per different temperature level.

| **Temp. level** | **No. of simulations** |
|---|---|
| 20 °C | 496 |
| 50 °C | 496 |
| 100 °C | 495 |
| 150 °C | 497 |
| 200 °C | 499 |
| 250 °C | 494 |

**Table 2.** Finite element mesh size vs average von Mises stress

| **Mesh size** | **Phase** | **Stress [MPa]** |
|---|---|---|
| 10×10×10 | Soft | 31.88 |
| 20×20×20 | Soft | 32.32 |
| 26×26×26 | Soft | 32.43 |
| 30×30×30 | Soft | 32.44 |
| 40×40×40 | Soft | 32.45 |
| 50×50×50 | Soft | 32.45 |
| 10×10×10 | Hard | 135.52 |
| 20×20×20 | Hard | 134.50 |
| 26×26×26 | Hard | 129.72 |
| 30×30×30 | Hard | 129.45 |
| 40×40×40 | Hard | 129.12 |
| 50×50×50 | Hard | 128.78 |

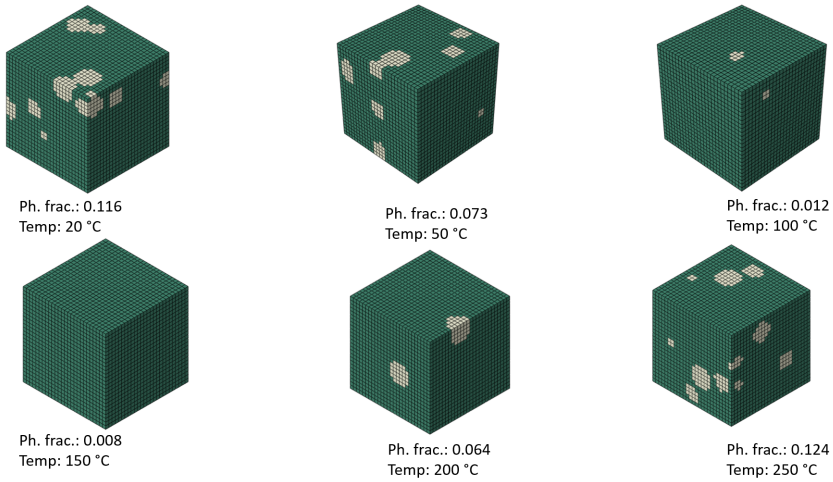


**Figure 4.** Visualization of the arrangement of the phases for an RVE for each temperature level.

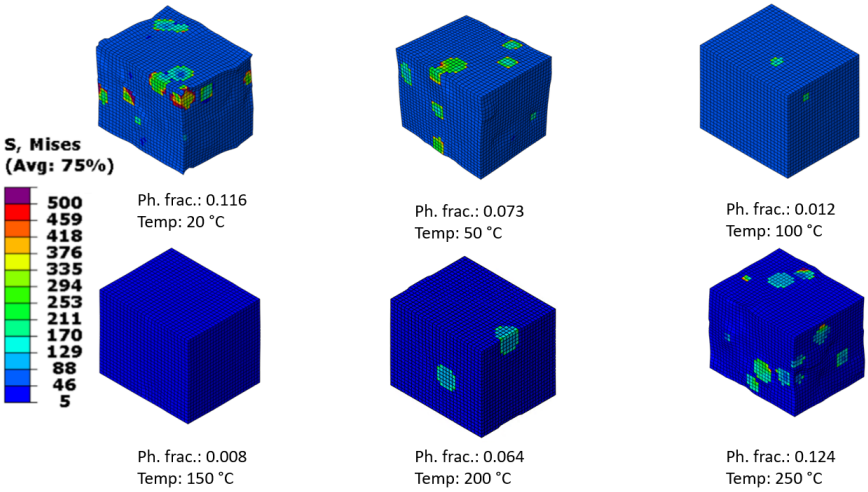


**Figure 5.** Resulting von Mises stress (MPa) for the RVEs in Fig. 4.

The output of interest was the response of true stress – true strain of the RVE for the given load. True stress – true strain response was averaged over each integration point of the RVE, and the corresponding strain and stress were recorded for each increment. This means that the mean RVE response for true stress – true strain was obtained from 20 uniformly distributed intervals. It should be noted that engineering stress refers to stress calculated based of the initial cross section area where contraction of the specimen during tensile test is not considered. However, in the whole research, true (Cauchy) stress is used which is calculated based on the actual cross section of the uniaxial tensile specimen is used. An example of the response for an RVE in Fig. 1 for the temperature of 20 °C is shown in Fig. 8. The von Mises stress was used for the equivalent stress, while the strain increment applied during loading was used for the strain output. This means that the simulation represents the macroscopic experimental uniaxial tensile test. It can be observed that the yield strength can be clearly seen in the graph as a point of departure from the initial

linear part of the curve. As the strain increases, the material begins develop plastic strain. A larger number of responses could be found in the Results section.

In addition, even other authors used similar mesh size on similar problems, a small study is performed to check the convergence of von Mises stress with the mesh size. A random RVE configuration is generated, the same for each mesh size, and stress was averaged as explained before, however, it was averaged through each phase separately. The results are checked for mesh sizes of 10×10×10, 20×20×20, 26×26×26, 30×30×30, 40×40×40, and 50×50×50 elements. The results are shown in Table 2. It could be observed that for both phases, maximum difference of stress value per phase is smaller than 6 MPa which could indicate that stress concentration is of minor importance here. In addition, it could be also observed that for the mesh size of 26×26×26 elements, the stress value starts to converge. Due to practical reasons of software's compatibility and computational time, the mesh size of 26×26×26 elements was chosen for this research.

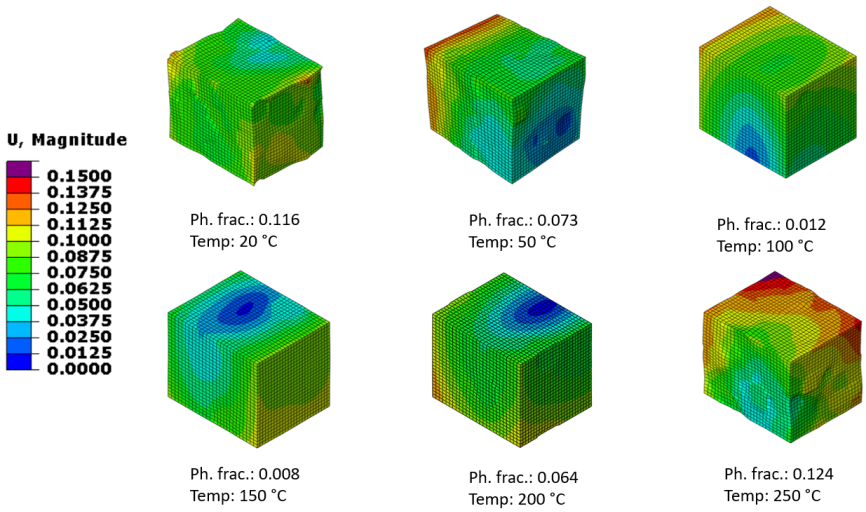


**Figure 6.** Resulting total displacement (mm) for the RVEs in Fig. 4.

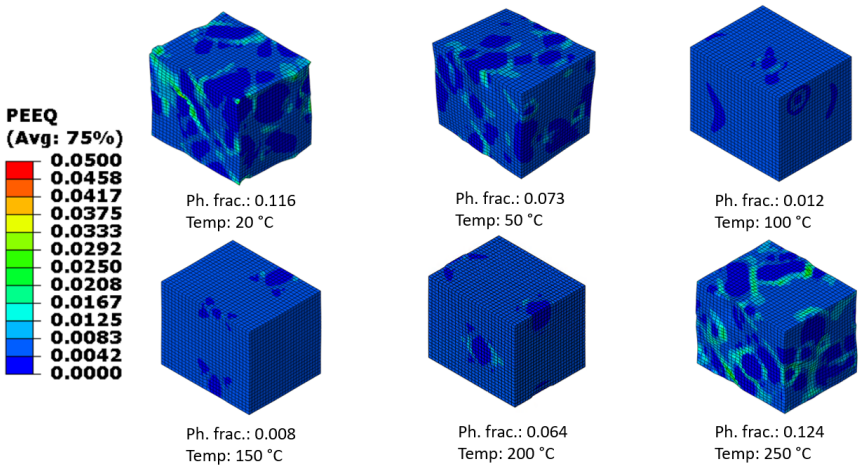


**Figure 7.** Resulting equivalent plastic strain for the RVEs in Fig. 4.

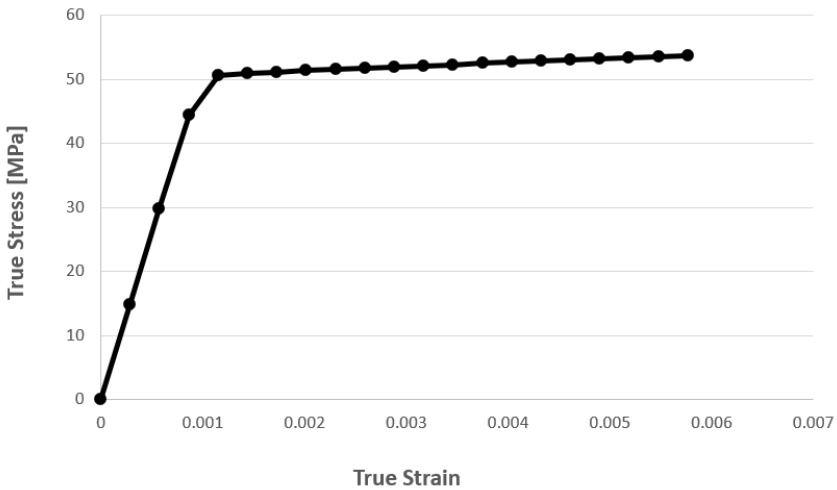


**Figure 8.** Example of the true stress – strain increment response for a RVE shown in Fig. 2. Temperature of the simulation is set at 20 °C.

## 2.3. *Overview of the ML Model*

ML algorithms can be broadly divided into two main types: shallow learning and deep learning (DL) algorithms [35]. It is well known that algorithms for shallow learning cannot be used for very complex tasks because they cannot learn a significantly large number of features. The DL algorithms, on the other hand, could, but their computational cost is higher. Many authors, including our previous results, have shown that DL algorithms such as CNN perform very well on a highly complex tasks [36–46]. Thus, it should be a reasonable decision to use CNN for the task at hand.

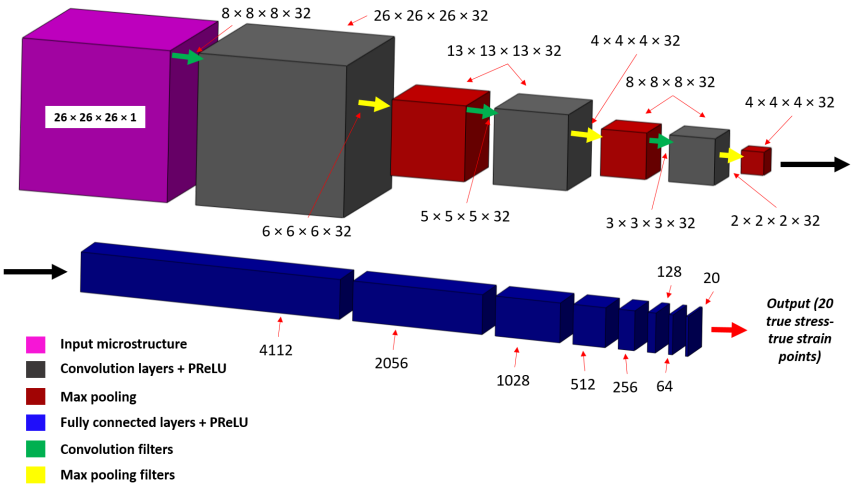


**Figure 9.** Schematic representation of the CNN architecture.

The CNN in the present case is based on a feed – forward (sequential) architecture. It is built of three blocks with 3D convolutional layers, Fig. 9. Parametric Rectified Linear Unit (PReLU) activation, max – pooling layer and batch normalization are used after each convolutional block.

For the first, second and third convolutional blocks, filter sizes of (8,8,8) × 32, (5,5,5) × 32, and (3,3,3) × 32 were used, respectively. Additionally, for the first, second, and third max – pooling layers, filter sizes of (6,6,6), (4,4,4), and (2,2,2) with strides 3 were used, respectively.

The last convolutional block is then flattened in a meta – layer of 512 neurons. After the meta – layer, fully connected layers of 4112, 2056, 1028, 512, 256, 128, and 64 neurons were used. Each layer is followed by the PReLU activation function and batch normalization. Finally, this layer is fully connected to the 20 logistic output neurons, which output the 20 true stress – true strain points. The CNN was trained with a learning rate of 0.0005 using an Adam optimizer. The model was trained with Tensorflow v2.6 and the Keras library on an Nvidia Quadro K2200 graphics card and converged within 300 epochs using mean squared error as validation loss metric. The training took approximately one hour. In addition, the model weights for each epoch were stored and the weights with the lowest validation loss were later selected to check the accuracy of the model. In this way, convergence instability was overcomed. The dataset for training was divided into the training set, the validation set, and the test set in a 60:20:20 ratio.

Unlike some other researches [2, 4, 6, 47], the model complexity in the present study was at enough level to show excellent performances even without dimension reduction techniques, see Results and Discussion section. Dimension reduction techniques could reduce the model input size and computational effort, however, the model performances could be compromised in this case. Since the training time of the model was approximately one hour what is reasonably short, dimensional reduction techniques were avoided in this study.

Thus, the input to the CNN was a 26×26×26 matrix that takes into account the information about the arrangement of the phases and the temperature level. It should be noted that the initial matrix of the material consists of zeros and ones (i.e., soft and hard phase), while the information about the temperature level was obtained by multiplying this matrix by the temperature. Thus, the temperature is directly included in the neural network. However, the model does not include some special hardening constants that are in some way temperature dependent. Instead, the stress - strain curves at selected temperatures for each phase are used. As a result, a classical constitutive model is not obtained, but the neural network takes this role, providing temperature hardening constitutive behavior of a two – phase material. The hyper – parameters of the model were calibrated manually via trial – and – error method, so there might exist a better performing model.

It should be emphasized that the ML model will reliably predict the mechanical behavior of a macroscopically isotropic solid under the boundary conditions that represent the uniaxial tensile tests. This is due to the randomness of the microstructure and the fact that the ML model captures the arrangement of the phases and can predict the behavior of any other RVE configuration. In this way, the model can be used for the same purpose as the results of the macroscopic experimental tensile test. However, the application of the present ML model to other boundary conditions, e.g., shear, should be done with caution.

In summary, the creation of the dataset consisted of automating the generation of the microstructures using DREAM.3D and Python. The output was in the form of the Abaqus input file taking into account the information about the arrangement of the phases within the RVE. Subsequently, a numerical simulation was performed using Abaqus software. The results of the simulation were true stress – true strain responses. ML model input matrices (phases arrangement and temperature) and vectors (output true stress – true strain response) were then generated using Python. A schematic representation of the process can be found in Fig. 10.

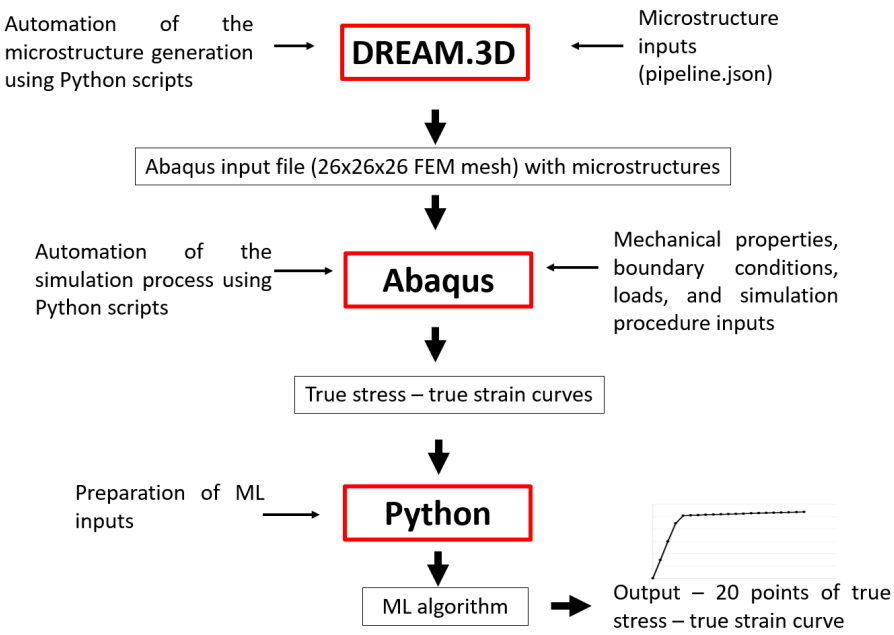


**Figure 10.** Schematic representation of the process.

## 3. Results and Discussion

The present section is divided into two subsections. In the first one, an analysis of the predictive accuracy of the model was tested using the test dataset with the six temperature levels. In the second one, the separately created dataset with the random temperature levels from 20 °C to 250 °C was tested. For simplicity, the dataset was trained on six temperature levels.

### 3.1. *Results for the Six Specific Temperature Levels*

First, the $R^2$ and mean squared error value of the model were evaluated using the 596 RVEs from the test set that were not used during training. The model performed excellently, achieving a $R^2$ score of 98.5 % and a mean squared error of 0.98 MPa. It should be noted that 596 predictions were made in a little less than one second. For comparison, this computational performance is extremely better than 596 FEA simulation runs in 150 hours. Next, the true stress – true strain responses from the FEA are compared to those predicted by the model. The comparison is performed for each temperature level for a random hard phase fraction. The results are shown in Fig. 11. It can be observed that as the temperature increases and the hard phase fraction decreases, the responses reach lower stress levels. The predicted curves at a temperature of 100 °C and 250 °C have some minor instabilities in the plastic part of the curve, but, this is to be expected since the model predicts each point with a small percentage of error. Thus, the responses are sensitive to temperature, hard phase fraction, and the arrangement of phases within the RVE.

In addition, the prediction accuracy of each response point is analyzed and compared with the FEA results. The prediction accuracy of the first two and the last two points of the curve are shown in Fig. 12, while the other points are available in the appendix. It can be observed that for strain point 2, two separate groups of values are highlighted in the graph. The reason for this is that the point is located in the middle part of the elastic region of the curve for which the values

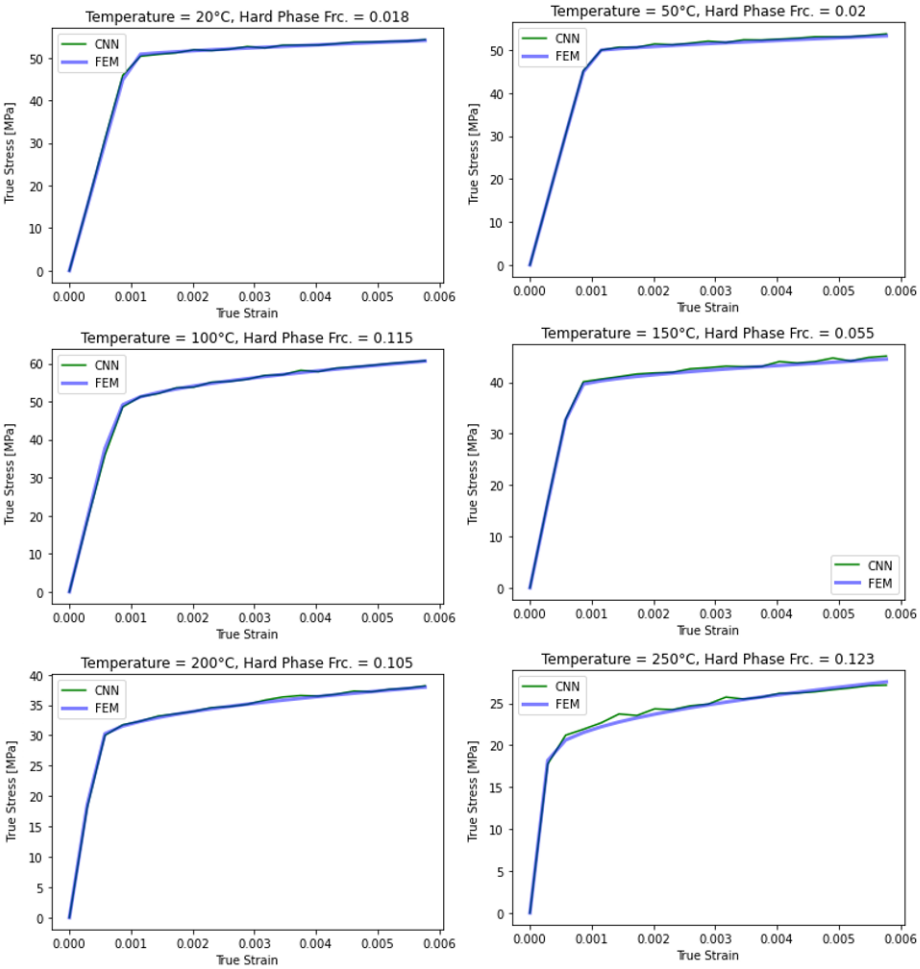


**Figure 11.** Comparison of the true stress – true strain responses predicted with CNN model and ones calculated with the finite element method.

**Table 3.** Dataset size vs mean squared error.

| **Dataset size** | **MSE [MPa]** |
|---|---|
| 100 % | 0.98 |
| 80 % | 1.28 |
| 60 % | 2.96 |
| 40 % | 4.88 |
| 20 % | 10.16 |

for the temperature of 250 °C are significantly lower than for the other temperature values. The maximum error between the calculated and the predicted value of the true stress from all strain points is 7.8 MPa, while the average error is 0.7 MPa. The calculated and predicted stress range for all points is between 14 MPa and 80 MPa. At the first three points, the general elastic trend of the true stress value increases rapidly, which is reasonable since in most RVEs the yield strength has not yet been reached. Thus, the stress value for the first point of the true stress – true strain curve ranges from 14 to 21 MPa, while the value for the last point ranges from 20 to 80 MPa.

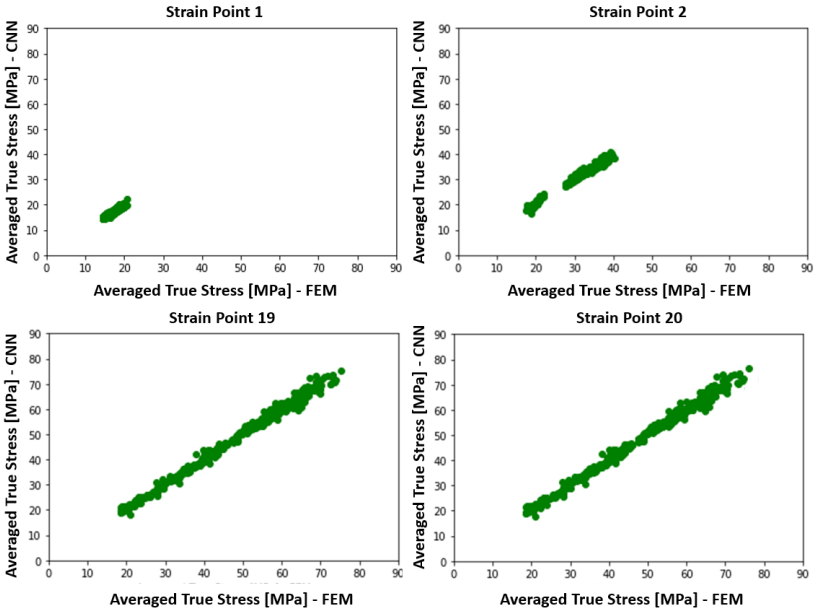


**Figure 12.** Comparison between predicted (CNN) and calculated (FEM) stress values for strain points 1, 2, 19 & 20 of the true stress – true strain curve for all temperatures combined.

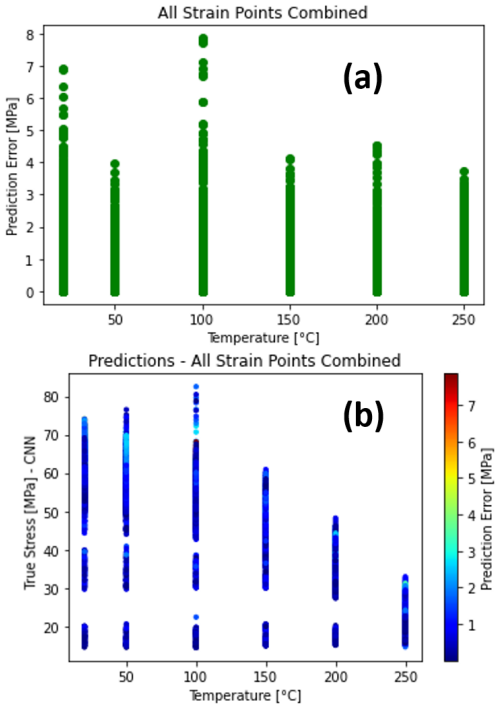


**Figure 13.** Comparison between predicted and calculated stress values for different temperatures for six temperature levels of all 20 points of the true stress – true strain curve: (a) prediction error versus temperature, (b) true stress versus temperature with colored prediction error.

The comparison between predicted and calculated stress values for different temperature levels is shown for all strain points, Fig. 13. It can be observed that the the trend of stress values decreases with increasing temperature. There are some exceptions, a stress value is slightly higher at a temperature of 100 °C than at 20 °C and 50 °C. This is related to the randomness of the dataset (i.e., for the temperature level of 100 °C, some RVEs with higher fractions of the hard phase and stiffer configuration were incidentally selected).

In addition, a comparison between the predicted and calculated stress values for different hard phase fractions is shown for all strain points, Fig. 14. It was also observed that the trend of stress values is higher with increasing hard phase fraction. The highest stress value is at a fraction of 0.125, and not at the maximum fraction (0.15). This indicates that the resulting true stress - true strain curve is also sensitive to the arrangement of the phases within the RVE, not only to the fraction value itself. Therefore, the 3D CNN captures arrangements of phases, phases fractions and temperature. It was also found that the prediction accuracy is not related to either the temperature or the fraction of the hard phase.

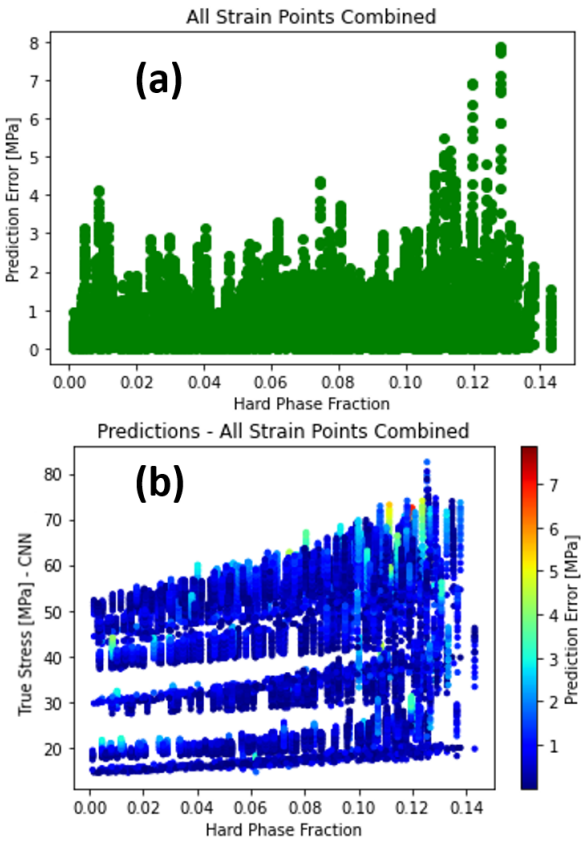


**Figure 14.** Comparison between predicted and calculated stress values for different hard phase fractions for six temperature levels of all 20 points of the true stress – true strain curve: (a) prediction error versus hard phase fraction, (b) true stress versus hard phase fraction with colored prediction error.

Furthermore, a short study is performed to investigate the impact of the dataset size on the results. The mean squared error is checked for the sizes of 80 %, 60 %, 40 %, and 20 % of the dataset. For simplicity, the same CNN configuration and training parameters as before were used for all trainings. The results are presented in Table 3. It can be noticed that the accuracy drops with decreasing of the dataset size, however, even with the dataset size of the 80 % and 60 % the mean squared error is rather small. However, with the dataset size of the 40 % and 20 % it starts increasing much more.

### 3.2. *Results for the Random Temperature Levels*

It is also important to show that the model can be used with a wide range of temperatures, not just the six specific temperature levels shown in the previous subsection. For this task, a dataset of 492 RVEs was created, covering randomly selected temperature in the range from 20 °C to 250 °C. The dataset was used as a basis for the model. The data set was created using the procedures described in the Methods section, as was the data set for the six temperature levels. Also, the same microstructural parameters and phases fraction randomly distribuded within the data set were used at all temperature levels. It should be noted that neither of the RVE arrangement used for this task were not used during training. For the 492 RVEs, the model performed excellently, achieving a $R^2$ score of 97.9 % and mean squared error of 1.9 MPa. It could be observed that the performances of the model were very similar as with the six specific temperature levels. In addition, there were no significant differences in computational efficiency compared to the dataset with six temperature levels.

Furthermore, the prediction accuracy of the response points is analyzed and compared with the FEA results. A similar trend as for the six temperature levels could be observed. Therefore, for the random temperature levels, only the plot containing all points combined is shown, Fig. 15. The maximum error between the calculated and predicted value of the true stress from all strain points is 7.1 MPa, while the average is 1 MPa. A similar trend to the six temperature levels was also observed. It can be concluded that temperature variations between the six temperature levels used for training do not affect the prediction accuracy for the respective temperature interval.

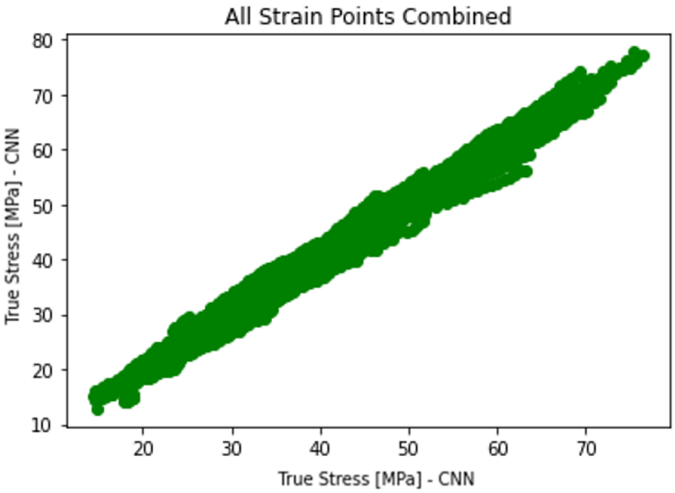


**Figure 15.** Comparison between predicted (CNN) and calculated (FEM) stress values for random temperature levels for different hard phase fractions of all 20 points of the true stress – true strain curve.

The comparison between predicted and calculated stress values for different temperature levels is shown for all strain points, Fig. 16. Again, the trend is observed that the stress value decreases with increasing temperature. The comparison between predicted and calculated stress values for different hard phase fractions is shown for all strain points, Fig. 17. It was also observed that the stress value is higher with increasing fraction. As in the previous subsection, the prediction accuracy does not depend on temperature or hard phase fraction.

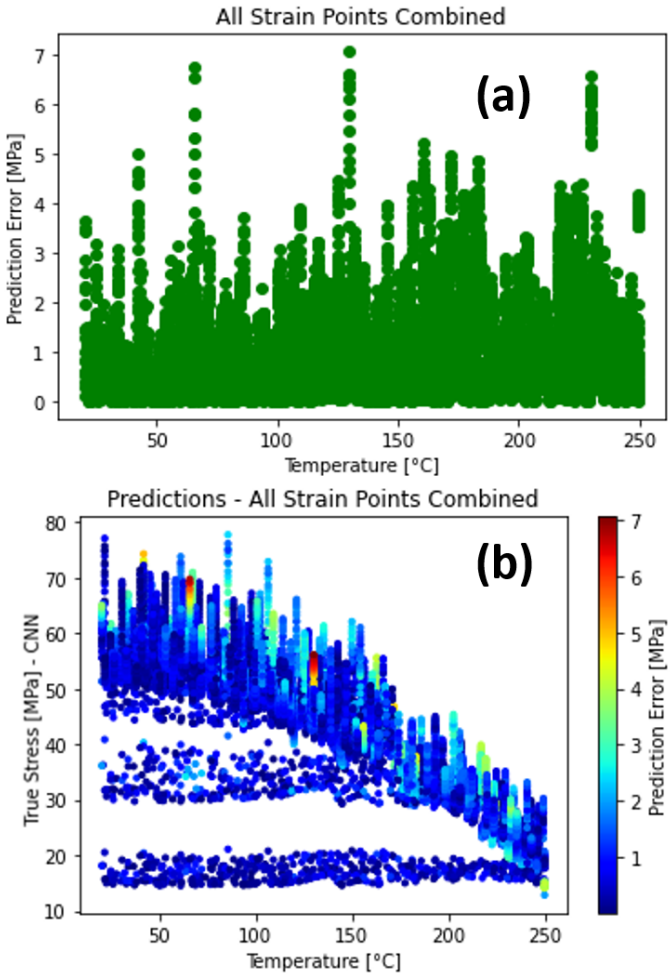


**Figure 16.** Comparison between predicted and calculated stress values for different temperatures for random levels of all 20 points of the true stress – true strain curve: (a) prediction error versus temperature, (b) true stress versus temperature with colored prediction error.

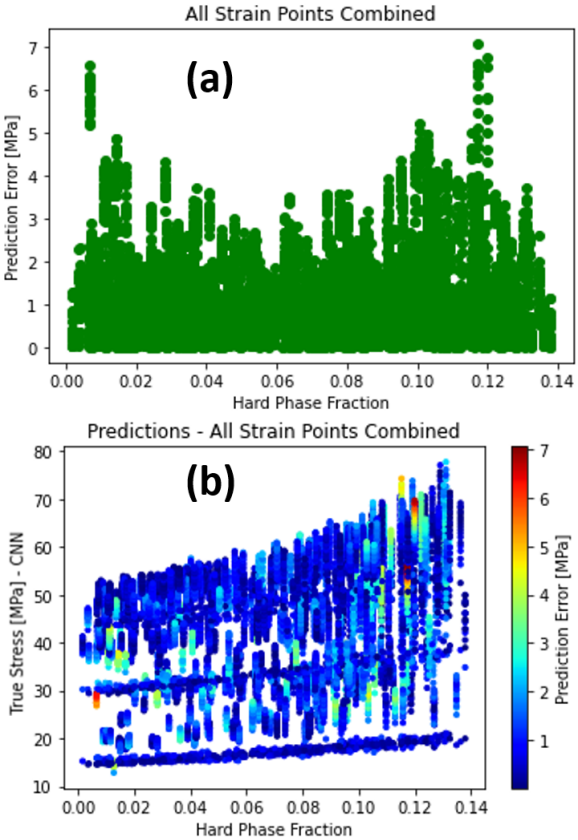


**Figure 17.** Comparison between predicted and calculated stress values for different hard phase fractions for random temperature levels of all 20 points of the true stress – true strain curve: (a) prediction error versus hard phase fraction, (b) true stress versus hard phase fraction with colored prediction error.

## 4. Conclusion

The present study confirms the hypothesis that the stress – strain curves at the different temperatures can be predicted from SPR by the ML methods. The present CNN model showed very high accuracy on the datased with six temperature levels. It achieved a $R^2$ of 98.5 % and mean squared error of 0.98 MPa for the test set of RVEs not used in training. The maximum error was 7.8 MPa, while the average error was 0.7 MPa. A similar trend in prediction accuracy is seen for the data set with random temperature values.

A more detailed investigation of the predictions of the individual points of the true stress – true strain is also provided. The investigation is performed for the case with six specific temperature levels. For the case with random temperature levels, all points were analyzed together. In addition, the influence of hard phase fraction and temperature on stress values and prediction accuracy is also investigated. In all tests, the model showed excellent prediction accuracy.

Future work should include realistic two – phase materials when the exact temperature – dependent properties of the materials in question are available. In this case, the effect of the microstructure arrangement within the RVE on the behavior of the component in service could be investigated. In addition, the future work could also include an extended example including shear loading.

## Conflicts of interest

The authors declare no competing financial interest.

## Author Contribution Statement

The manuscript was written through contributions of all authors. All authors have given approval to the final version of the manuscript.

## Acknowledgments

All the support is gratefully acknowledged.

## References

[1] X. Li, Z. Liu, S. Cui, C. Luo, C. Li, Z. Zhuang, "Predicting the effective mechanical property of heterogeneous materials by image based modeling and deep learning", *Comput. Methods Appl. Mech. Eng.* **347** (2019), p. 735-753.

[2] J. Jung, J. I. Yoon, H. K. Park, J. Y. Kim, H. S. Kim, "An efficient machine learning approach to establish structure-property linkages", *Comput. Mater. Sci.* **156** (2019), p. 17-25.

[3] H. Zhang, Z. Guo, H. Hu, G. Zhou, Q. Liu, Y. Xu, Q. Qian, D. Dai, "A novel structure-property relationship model based on machine learning", *Model. Simul. Mat. Sci. Eng.* **28** (2020), no. 3, article no. 035002.

[4] M. I. Latypov, S. R. Kalidindi, "Data-driven reduced order models for effective yield strength and partitioning of strain in multiphase materials", *J. Comput. Phys.* **346** (2017), p. 242-261.

[5] Z. Yang, Y. C. Yabansu, R. Al-Bahrani, W.-k. Liao, A. N. Choudhary, S. R. Kalidindi, A. Agrawal, "Deep learning approaches for mining structure-property linkages in high contrast composites from simulation datasets", *Comput. Mater. Sci.* **151** (2018), p. 278-287.

[6] A. Cecen, H. Dai, Y. C. Yabansu, S. R. Kalidindi, L. Song, "Material structure-property linkages using three-dimensional convolutional neural networks", *Acta Mater.* **146** (2018), p. 76-84.

[7] Y. Wang, M. Zhang, A. Lin, A. Iyer, A. S. Prasad, X. Li, Y. Zhang, L. S. Schadler, W. Chen, L. C. Brinson, "Mining structure–property relationships in polymer nanocomposites using data driven finite element analysis and multi-task convolutional neural networks", *Mol. Syst. Des. Eng.* **5** (2020), no. 5, p. 962-975.

[8] Z. Liu, C. Wu, M. Koishi, "Transfer learning of deep material network for seamless structure–property predictions", *Comput. Mech.* **64** (2019), no. 2, p. 451-465.

[9] S. Kotha, D. Ozturk, S. Ghosh, "Parametrically homogenized constitutive models (PHCMs) from micromechanical crystal plasticity FE simulations, part I: Sensitivity analysis and parameter identification for Titanium alloys", *Int. J. Plast.* **120** (2019), p. 296-319.

[10] A. Frankel, C. Safta, C. Alleman, R. Jones, "Mesh-based graph convolutional neural network models of processes with complex initial states", https://arxiv.org/abs/2107.00090, 2021.

[11] C. Yang, Y. Kim, S. Ryu, G. X. Gu, "Prediction of composite microstructure stress-strain curves using convolutional neural networks", *Mater. Des.* **189** (2020), article no. 108509.

[12] K. Jiang, Q. Han, Y. Bai, X. Du, "Data-driven ultimate conditions prediction and stress-strain model for FRP-confined concrete", *Compos. Struct.* **242** (2020), article no. 112094.

[13] J. Wen, Q. Zou, Y. Wei, "Physics-driven machine learning model on temperature and time-dependent deformation in lithium metal and its finite element implementation", *J. Mech. Phys. Solids* **153** (2021), article no. 104481.

[14] D. Versino, A. Tonda, C. A. Bronkhorst, "Data driven modeling of plastic deformation", *Comput. Methods Appl. Mech. Eng.* **318** (2017), p. 981-1004.

[15] G. Kronberger, E. Kabliman, J. Kronsteiner, M. Kommenda, "Extending a physics-based constitutive model using genetic programming", *Applications in Engineering Science* **9** (2022), article no. 100080.

[16] C. Gebhardt, T. Trimborn, F. Weber, A. Bezold, C. Broeckmann, M. Herty, "Simplified ResNet approach for data driven prediction of microstructure-fatigue relationship", *Mech. Mater.* **151** (2020), article no. 103625.

[17] B. P. Croom, M. Berkson, R. K. Mueller, M. Presley, S. Storck, "Deep learning prediction of stress fields in additively manufactured metals with intricate defect networks", *Mech. Mater.* **165** (2022), article no. 104191.

[18] A. Bhaduri, A. Gupta, L. Graham-Brady, "Stress field prediction in fiber-reinforced composite materials using a deep learning approach", *Compos. B. Eng.* **238** (2022), article no. 109879.

[19] C. McElfresh, C. Roberts, S. He, S. Prikhodko, J. Marian, "Using machine-learning to understand complex microstructural effects on the mechanical behavior of Ti-6Al-4V alloys", *Comput. Mater. Sci.* **208** (2022), article no. 111267.

[20] C. Herriott, A. D. Spear, "Predicting microstructure-dependent mechanical properties in additively manufactured metals with machine- and deep-learning methods", *Comput. Mater. Sci.* **175** (2020), article no. 109599.
[21] C. Rao, Y. Liu, "Three-dimensional convolutional neural network (3D-CNN) for heterogeneous material homogenization", *Comput. Mater. Sci.* **184** (2020), article no. 109850.
[22] D. W. Abueidda, M. Almasri, R. Ammourah, U. Ravaioli, I. M. Jasiuk, N. A. Sobh, "Prediction and optimization of mechanical properties of composites using convolutional neural networks", *Compos. Struct.* **227** (2019), article no. 111264.
[23] S. Ye, B. Li, Q. Li, H.-P. Zhao, X.-Q. Feng, "Deep neural network method for predicting the mechanical properties of composites", *Appl. Phys. Lett.* **115** (2019), no. 16, article no. 161901.
[24] A. D. Casey, S. F. Son, I. Bilionis, B. C. Barnes, "Prediction of Energetic Material Properties from Electronic Structure Using 3D Convolutional Neural Networks", *J. Chem. Inf. Model.* **60** (2020), no. 10, p. 4457-4473.
[25] M. A. Groeber, M. A. Jackson, "DREAM.3D: a digital representation environment for the analysis of microstructure in 3D", *Integr. Mater. Manuf. Innov.* **3** (2014), no. 1, p. 56-72.
[26] S. Balasivanandha Prabu, L. Karunamoorthy, "Microstructure-based finite element analysis of failure prediction in particle-reinforced metal-matrix composite", *J. Mater. Process. Technol.* **207** (2008), no. 1-3, p. 53-62.
[27] A. B. Phillion, S. L. Cockcroft, P. D. Lee, "Predicting the constitutive behavior of semi-solids via a direct finite element simulation: application to AA5182", *Model. Simul. Mat. Sci. Eng.* **17** (2009), no. 5, article no. 055011.
[28] K. Kim, B. Forest, J. Geringer, "Two-dimensional finite element simulation of fracture and fatigue behaviours of alumina microstructures for hip prosthesis", *Proc. Inst. Mech. Eng. H.* **225** (2011), no. 12, p. 1158-1168.
[29] S. Patel, R. Vaish, N. Sinha, C. R. Bowen, "Finite element analysis of the microstructure of AlN-TiN composites", *Strain* **50** (2014), no. 3, p. 250-261.
[30] S. Kench, S. J. Cooper, "Generating three-dimensional structures from a two-dimensional slice with generative adversarial network-based dimensionality expansion", *Nat. Mach. Intell.* **3** (2021), no. 4, p. 299-305.
[31] G. Al Kassem, "Micromechanical material models for polymer composites through advanced numerical simulation techniques", PhD Thesis, RWTH Aachen University, Aachen, Germany, 2010.
[32] V. G. Kouznetsova, M. G. D. Geers, W. A. M. Brekelmans, "Multi-scale constitutive modelling of heterogeneous materials with a gradient-enhanced computational homogenization scheme", *Int. J. Numer. Methods Eng.* **54** (2002), no. 8, p. 1235-1260.
[33] M. G. D. Geers, V. G. Kouznetsova, W. A. M. Brekelmans, "Multi-scale computational homogenization: Trends and challenges", *J. Comput. Appl. Math.* **234** (2010), no. 7, p. 2175-2182.
[34] M. Smith, "ABAQUS/Standard User's Manual, Version 6.9", 2009.
[35] J. Wei, X. Chu, X.-Y. Sun, K. Xu, H.-X. Deng, J. Chen, Z. Wei, M. Lei, "Machine learning in materials science", *InfoMat* **1** (2019), no. 3, p. 338-358.
[36] C. Herriott, A. D. Spear, "Predicting microstructure-dependent mechanical properties in additively manufactured metals with machine-and deep-learning methods", *Comput. Mater. Sci.* **175** (2020), article no. 109599.
[37] M. Ragone, V. Yurkiv, B. Song, A. Ramsubramanian, R. Shahbazian-Yassar, F. Mashayek, "Atomic column heights detection in metallic nanoparticles using deep convolutional learning", *Comput. Mater. Sci.* **180** (2020), article no. 109722.
[38] A. Khan, D.-K. Ko, S. C. Lim, H. S. Kim, "Structural vibration-based classification and prediction of delamination in smart composite laminates using deep learning neural network", *Compos. B. Eng.* **161** (2019), p. 586-594.
[39] S. M. Azimi, D. Britz, M. Engstler, M. Fritz, F. Mücklich, "Advanced steel microstructural classification by deep learning methods", *Sci. Rep.* **8** (2018), no. 1, article no. 2128.
[40] X. Li, Y. Zhang, H. Zhao, C. Burkhart, L. C. Brinson, W. Chen, "A transfer learning approach for microstructure reconstruction and structure-property predictions", *Sci. Rep.* **8** (2018), no. 1, article no. 13461.
[41] B. L. DeCost, B. Lei, T. Francis, E. A. Holm, "High Throughput Quantitative Metallography for Complex Microstructures Using Deep Learning: A Case Study in Ultrahigh Carbon Steel", *Microsc. Microanal.* **25** (2019), no. 1, p. 21-29.
[42] M. K. Ferguson, A. Ronay, Y.-T. T. Lee, K. H. Law, "Detection and segmentation of manufacturing defects with convolutional neural networks and transfer learning", *Smart Sustain Manuf Syst.* **2** (2018).
[43] M. Rautela, A. Huber, J. Senthilnath, S. Gopalakrishnan, "Inverse characterization of composites using guided waves and convolutional neural networks with dual-branch feature fusion", *Mech. Adv. Mater. Struct.* (2021).
[44] S. Javadi, A. Maghami, S. M. Hosseini, "A deep learning approach based on a data-driven tool for classification and prediction of thermoelastic waves band structures for phononic crystals", *Mech. Adv. Mater. Struct.* **29** (2021), no. 27, p. 6612-6625.
[45] F. Nikolić, I. Štajduhar, M. Čanađija, "Casting Microstructure Inspection Using Computer Vision: Dendrite Spacing in Aluminum Alloys", *Metals* **11** (2021), no. 5, p. 756.
[46] F. Nikolić, I. Štajduhar, M. Čanađija, "Casting Defects Detection in Aluminum Alloys Using Deep Learning: a Classification Approach", *Inter. Metalcast.* (2022).
[47] G. Ammasai Sengodan, "Prediction of two-phase composite microstructure properties through deep learning of reduced dimensional structure-response data", *Compos. B. Eng.* **225** (2021), article no. 109282.